

# Journal of Materials Chemistry A

Accepted Manuscript



This is an *Accepted Manuscript*, which has been through the Royal Society of Chemistry peer review process and has been accepted for publication.

*Accepted Manuscripts* are published online shortly after acceptance, before technical editing, formatting and proof reading. Using this free service, authors can make their results available to the community, in citable form, before we publish the edited article. We will replace this *Accepted Manuscript* with the edited and formatted *Advance Article* as soon as it is available.

You can find more information about *Accepted Manuscripts* in the [Information for Authors](#).

Please note that technical editing may introduce minor changes to the text and/or graphics, which may alter content. The journal's standard [Terms & Conditions](#) and the [Ethical guidelines](#) still apply. In no event shall the Royal Society of Chemistry be held responsible for any errors or omissions in this *Accepted Manuscript* or any consequences arising from the use of any information it contains.



Journal Name

ARTICLE

## On the nature of niobium substitution in niobium doped titania thin films by AACVD and its impact on electrical and optical properties

Received 00th January 20xx,  
Accepted 00th January 20xx

DOI: 10.1039/x0xx00000x

www.rsc.org/

A. J. Gardecka<sup>a,b</sup>, G. Goh K.L.<sup>b</sup>, G. Sankar<sup>a</sup> and I. P. Parkin<sup>a\*</sup>

Niobium doped TiO<sub>2</sub> thin films were deposited on silica coated glass substrate using aerosol assisted chemical vapour deposition (AACVD) from hexane solution, at 500°C. The as-deposited films appeared blue, were transparent in the visible, were reflective in the IR region at around 30% and were electrically conductive ( $n = 1.23 \times 10^{19} \text{ cm}^{-3}$ ,  $\mu = 18.9 \text{ cm}^2/\text{Vs}$ ,  $\square = 120 \text{ } \Omega/\square$ ). The structure of the films was investigated using XRD, Raman spectroscopy, XPS and X-ray absorptionspectroscopy (XAS). No visible phase segregation was found by XRD nor by Raman, though analysis of the Nb k-edge using XANES and EXAFS revealed the presence of niobium both incorporated into the titanium dioxide lattice as well as present in the form of Nb<sub>2</sub>O<sub>5</sub>. The high resolution TEM imaging showed sub 4nm Nb<sub>2</sub>O<sub>5</sub> crystals within the lattice. This work questions the solubility limit of niobium in the TiO<sub>2</sub> lattice and suggests previous literature on Nb-doped TiO<sub>2</sub> may have overestimated the degree of niobium substitution.

### Introduction

Titanium dioxide (TiO<sub>2</sub>) is commonly used for its UV-promoted photocatalytic and self-cleaning properties. Mechanical durability, transparency, relatively low cost, resistance to photo-corrosion,<sup>1</sup> high photo-activity and photo-induced super-hydrophilicity make titania thin films a desirable product for glass coating.<sup>2,3</sup> These properties allow better surface water-wetting of glass windows, which results in removal of the dirt without leaving stains, and enhanced photodegradation of organic residues and bacteria. Indeed a number of commercial self cleaning window glasses are in the market including NSG Activ<sup>TM</sup>, Saint Goban Bioclean<sup>TM</sup>, PPG Sunclean<sup>TM</sup> and Viridian Neat<sup>TM</sup> glass. This industry is worth over \$1.5B per annum at the distributor level- and over 2000 installation companies are registered to use the products.<sup>4</sup>

Despite working well as a solar driven photocatalyst, the intrinsic band gap of TiO<sub>2</sub> is 3.2 eV –corresponding to light of less than 390 nm. The bulk resistivity of TiO<sub>2</sub> is about  $1 \times 10^6 \text{ } \Omega$ ; therefore TiO<sub>2</sub> is classified as a poor semiconductor.<sup>5</sup> The functional properties of titania can be readily adapted by introducing aliovalent cations that form donors and acceptors, as well as by changing its oxygen sub-stoichiometry.

The main characteristic of transparent conducting oxides (TCO's) are the large values of electrical conductivity (For example, aluminium doped ZnO (AZO) display electrical

resistivity of order  $10^{-5} \text{ } \Omega\text{-cm}$ )<sup>6</sup>, while maintaining high transmittance in the visible spectrum of light.<sup>7,8</sup> Currently used TCO's rely on the intrinsic vacancies within the metal oxides structures, using extrinsic dopants in order to generate n-type conduction, such materials include tin doped indium oxide (ITO), fluorine doped tin oxide (FTO) and aluminium and gallium doped zinc oxides (AZO and GZO).<sup>9-11</sup>

Other promising materials are carbon based nanostructures such as graphene and carbon nanotubes (CNT's) thin films. The nanonet films assembled of few layers of CNT's overlapping in the way that they create a network of possible electrically conductive channels, leading to metal-like electrical conductivity and an excellent mechanical robustness.<sup>12-14</sup>

Niobium doped titania films have recently been also found to be promising competition for ZnO films doped with gallium or aluminum as well as indium tin oxide for application as TCO's and contact layers for thin films solar cells, optoelectronics applications<sup>13,14</sup> and photoinduced water splitting.<sup>17</sup> Niobium doped titania films with the required low resistivity to function as TCO materials have been formed by pulsed laser deposition (PLD)<sup>16</sup>. Theoretical studies have also indicated that niobium doped titania should be a good candidate for a TCO material. In this paper in addition to traditional characterisation methods, we report XAFS studies on the different levels of niobium doped titania thin films and the effect of phase segregation on the electrical and optical properties of thin films. The processing method we employed included making an aerosol of precursors dispersed in a hexane mist. Such a solvent system is compatible with commercial glass manufacture. Furthermore the XAFS studies surprisingly show a presence of Nb<sub>2</sub>O<sub>5</sub> component, confirmed by high resolution TEM analysis. The presence of this was undetectable by

<sup>a</sup> Materials Chemistry Centre, Department of Chemistry, University College London, 20 Gordon Street, London WC1H 0AJ, UK E-mail: [i.p.parkin@ucl.ac.uk](mailto:i.p.parkin@ucl.ac.uk)

<sup>b</sup> Institute of Materials Research and Engineering, Agency for Science, Technology and Research (A\*STAR), 3, Research Link, Singapore 117602.

common characterisation techniques- including XRD and Raman. This work calls into question the actual solubility limit, reported in literature as 40% by mole fraction<sup>2,18-20</sup> of Nb in the anatase titanium dioxide lattice- at least as prepared by AACVD using hexane as a solvent.

## Experimental

All chemicals used in this experiment were purchased from Sigma Aldrich Chemical Co. and used without further purification; 2 g of technical grade titanium (IV) ethoxide, (0-10 atom % Nb:Ti) 99.95% niobium (V) ethoxide, 25 mL of hexane. Nitrogen (oxygen free) was provided by BOC. The precursor flow was kept at  $0.6 \text{ l min}^{-1}$ . Deposition was carried on a  $15 \text{ cm} \times 3.5 \text{ cm} \times 0.3 \text{ cm}$  standard float glass coated with a 50 nm layer of  $\text{SiO}_2$  to prevent ion migration from the glass<sup>21</sup> supplied by Pilkington NSG Group. Films were deposited in a cold wall reactor in the  $\text{N}_2$  atmosphere, the temperature of the substrate was  $500^\circ\text{C}$  during the entire deposition, and then cooled to the room temperature.

For identification of the crystal structure and preferred orientation growth of the film X-Ray diffraction (XRD) was used. This was carried out on a *Bruker GADDS D8* diffractometer with a  $\text{Cu K}\alpha$  X-Ray source and readings were taken over the  $10^\circ < 2\theta < 66^\circ$  range. To confirm the phase of the film a *Reinshaw 1000 Invia* Raman spectrometer was used under ambient conditions with an Ar laser source (514.5 nm) over the  $100\text{-}1500 \text{ cm}^{-1}$  wavelength range. XAS spectra of as-deposited samples at the Nb (18990 eV) *K*-edges were taken at the B18 beamline of the Diamond Light Source. Obtained data was normalized and fitted using Athena and Artemis software and were calculated on the basis of anatase  $\text{TiO}_2$  and  $\text{Nb}_2\text{O}_5$  structures. Linear combination fit (LCF) of normalized XANES spectra was calculated with  $\text{Ti}_{0.97}\text{Nb}_{0.03}\text{O}_2$  thin film and  $\text{Nb}_2\text{O}_5$ , as reference materials. To determine the structural parameters of investigated samples related to the niobium site, multiple shell fitting was carried out at the *k*-range  $2.8 - 12.1 \text{ \AA}^{-1}$ , *R*-range  $1.3 - 4 \text{ \AA}$  and *k*-weight equals 2. Transmittance- Reflectance (T-R) spectra were taken against an air background using a *Perkin Elmer Fourier Transform Lambda 950* UV-vis spectrometer at a wavelength range of 200-2500 nm. Film thickness was derived from the transmittance spectrum *via Swanepoel's* method. Energy dispersive X-ray spectroscopy (EDX- obtained by using a *JEOL JSM-6301F Field Emission SEM*) was used to determine the Nb:Ti atomic ratio on the C-coated samples. Lattice structural information and EDX mapping were examined with *JEOL 2100 TEM*. Measurements of surface composition and the state of elements were carried out using a *Thermo Scientific K-Alpha* X-ray photoelectron spectrometer (XPS) with a monochromatic Al-K $\alpha$  source. Results were then fitted using *CasaXPS* software with the binding energies suited to carbon (285 eV). UV-vis transmittance spectra were taken after irradiation with 365 nm light until complete decomposition of the dye. Charge carrier concentration ( $n / \text{cm}^{-3}$ ), charge carrier mobility ( $\mu / \text{cm}^2 \text{ V}^{-1} \text{ s}^{-1}$ ), bulk resistivity ( $\rho / \Omega \text{ cm}$ ) and sheet resistance ( $R_{sh} / \Omega \square^{-1}$ ) were measured at room temperature on an *Escopia HMS-*

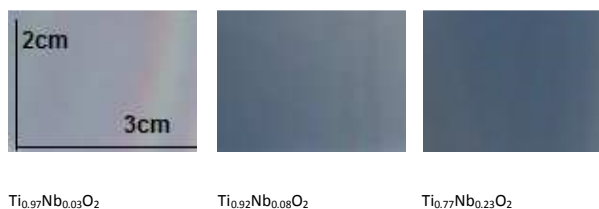


Figure 1. Images showing niobium doped titania thin films deposited by AACVD image size is ca 10 cm by 5 cm. The photograph was taken against white background.

3000 set up in the Van der Pauw configuration. Measurements were carried out using a current of  $1 \mu\text{A}$  and a 0.58 T permanent magnet on  $\approx 1 \times 1 \text{ cm}$  squares with silver paint (Agar Scientific) used as ohmic contacts, integrity of which was tested prior to measurements.

## Results and discussion

Aerosol assisted chemical vapour deposition (AACVD) of Nb-doped  $\text{TiO}_2$  films was achieved on glass substrates from a mix of  $[\text{Ti}(\text{OEt})_4]$  and  $[\text{Nb}(\text{OEt})_5]$  in hexane at  $500^\circ\text{C}$ . The as-deposited films were blue in colour and the intensity of the colour increased with niobium incorporation (Figure 1.). All the films deposited uniformly on the glass plate, were adherent to the substrate, passing the Scotch tape test, were insoluble in common solvents and were stable in air for over a year.

X-ray diffraction showed that the only crystalline phase present in all the films is the anatase form of  $\text{TiO}_2$ . Surprisingly the XRD patterns reveal strong preferred orientation within the deposited films. In anatase powder and 0% Nb: $\text{TiO}_2$  the most intense reflection corresponds to the (101) plane, which decreases in intensity with niobium concentration in the initial starting solution. The apparent niobium concentration in the films also correlates with an increase in intensity of the (105) reflection. No other titania phases (brookite, rutile) were

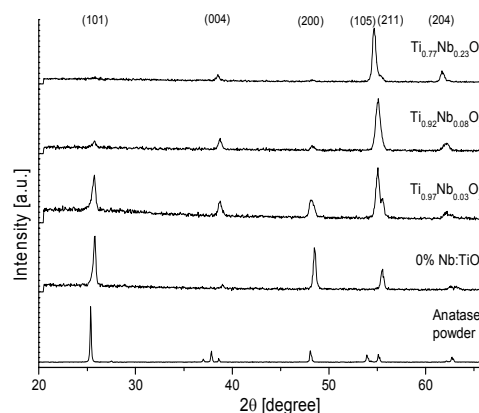


Figure 2. XRD pattern of anatase powder and Nb doped titania films prepared by AACVD on silica coated glass. The anatase reflection positions with appropriate values (h k l) are shown in brackets.

Journal Name

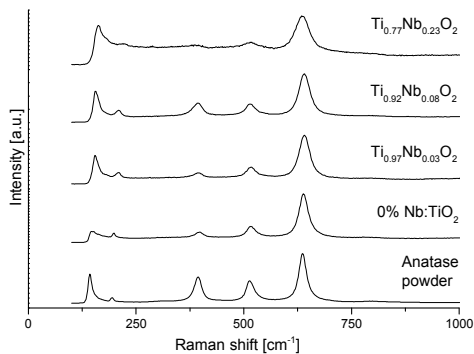


Figure 3. Raman spectra of anatase powder and as-deposited Nb doped titania films on silica coated glass.

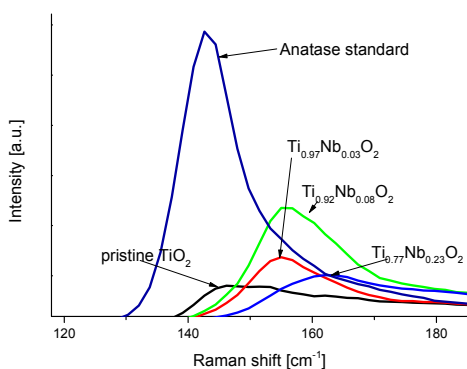


Figure 4. Shift of  $E_g$  band of niobium doped  $\text{TiO}_2$  and pristine titania films formed from the AACVD compared to anatase powder

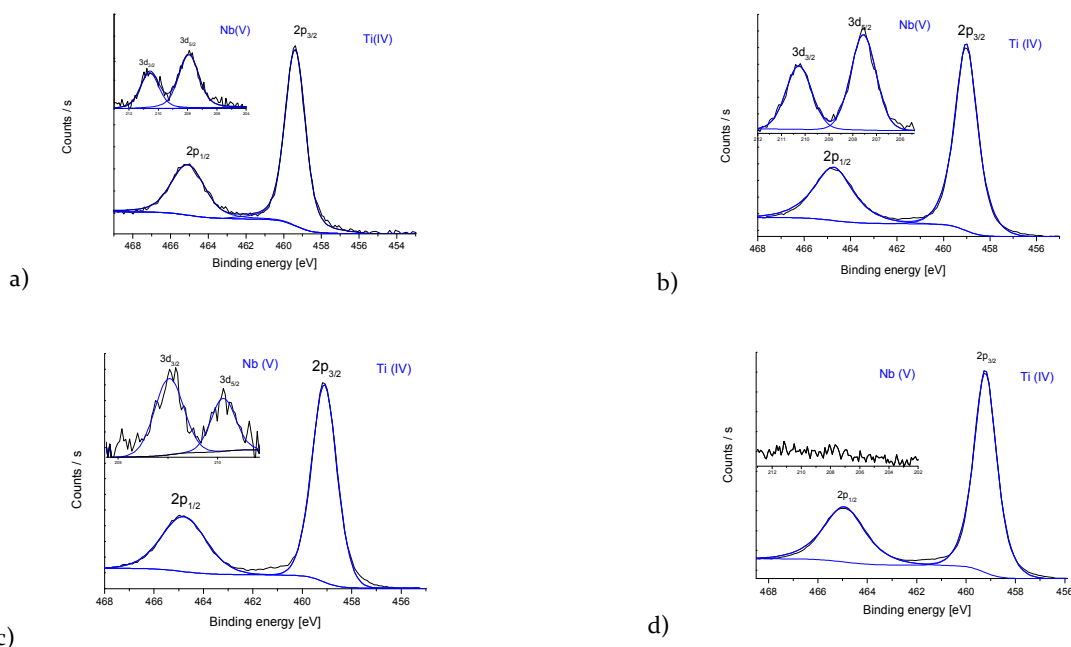


Figure 6. XPS spectra of as deposited a)  $\text{Ti}_{0.97}\text{Nb}_{0.03}\text{O}_2$  b)  $\text{Ti}_{0.92}\text{Nb}_{0.08}\text{O}_2$  c)  $\text{Ti}_{0.77}\text{Nb}_{0.23}\text{O}_2$  d) pristine  $\text{TiO}_2$  thin films in the titanium 2p region (inserts show niobium 3p region).

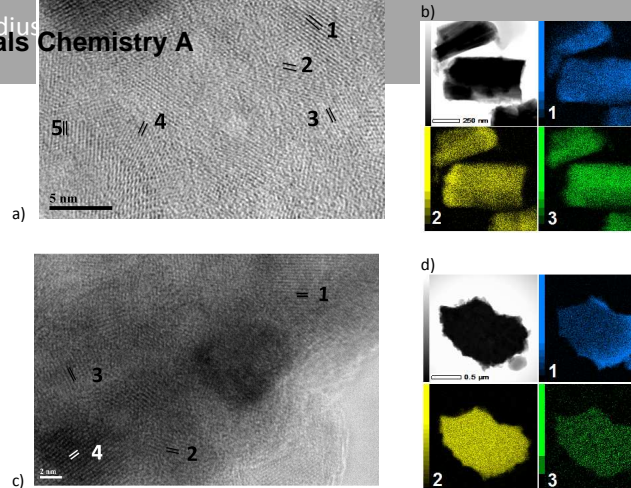


Figure 5. TEM picture of a)  $\text{Ti}_{0.77}\text{Nb}_{0.23}\text{O}_2$  (number 1 correlates to  $\text{TiO}_2$   $d_{101}=3.55\pm 0.01\text{\AA}$ , 2-  $d_{112}=2.34\pm 0.02\text{\AA}$ , 3-  $d_{004}=2.38\pm 0.01\text{\AA}$ , 4-  $d_{103}=2.43\pm 0.01\text{\AA}$  and 5 for  $\text{Nb}_2\text{O}_5$   $d=3.08\pm 0.01\text{\AA}$ ) c)  $\text{Ti}_{0.97}\text{Nb}_{0.03}\text{O}_2$  (number 1 correlates to  $\text{TiO}_2$   $d_{101}=3.55\pm 0.01\text{\AA}$ , 2-  $d_{112}=2.34\pm 0.02\text{\AA}$ , 3-  $d_{004}=2.38\pm 0.01\text{\AA}$ , 4-  $d_{105}=1.69\pm 0.01\text{\AA}$ ), b,d) corresponding elemental mapping of O-K (1), Ti-K (2) and Nb-L (3).

found neither could niobium oxide be observed in the XRD pattern or in the Raman spectrum (Fig.3). The Raman patterns are fully consistent with the formation of only the anatase form of  $\text{TiO}_2$ . Notably the peak at  $143\text{ cm}^{-1}$  in pure anatase is shifted to higher energy with niobium doping (Fig. 4), which was also observed by Fehse *et al.*<sup>22</sup> and is attributed to the change in O-Ti-O bending vibration. This is also consistent with previous studies based on W-doping into  $\text{TiO}_2$ .<sup>23</sup> In accordance with the work of Sheppard *et al.*<sup>1</sup> the titania lattice expands in direct proportion with the amount of niobium concentration in the film. The Raman pattern peaks tend to become broader with niobium content. Despite this broadening, no niobium oxide phase could be detected by Raman.<sup>24,25</sup>

Table 1. Results of Nb K-edge EXAFS analysis. R-factor for  $\text{Ti}_{0.97}\text{Nb}_{0.03}\text{O}_2 = 0.0198$ , for  $\text{Ti}_{0.93}\text{Nb}_{0.07}\text{O}_2 + 10.8\% \text{Nb}_2\text{O}_5 = 0.0078$  (N- coordination number, R- interatomic distance,  $\sigma^2$ - mean square relative displacement).

Sample	Nb O			Nb Ti <sub>1</sub>			Nb Ti <sub>2</sub>		
	R [Å]	N	$\sigma^2$ [Å]	R [Å]	N	$\sigma^2$ [Å]	R [Å]	N	$\sigma^2$ [Å]
$\text{Ti}_{0.97}\text{Nb}_{0.03}\text{O}_2$	1.98	6	0.001	3.13	4	0.004	3.85	4	0.007
$\text{Ti}_{0.92}\text{Nb}_{0.08}\text{O}_2$	1.99	6	0.001	3.13	4	0.005	3.86	4	0.009

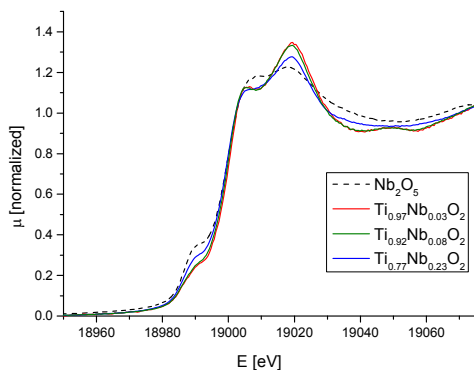


Figure 7. Normalised XANES  $\text{Nb}_2\text{O}_5$ ,  $\text{Ti}_{0.97}\text{Nb}_{0.03}\text{O}_2$ ,  $\text{Ti}_{0.92}\text{Nb}_{0.08}\text{O}_2$  and  $\text{Ti}_{0.77}\text{Nb}_{0.23}\text{O}_2$  thin films.

Close TEM examination of each crystallites show that the d-spacing of most of them is consistent with anatase, except small nanocrystallites with d-spacing  $3.08 \pm 0.01 \text{ \AA}$  in the  $\text{Ti}_{0.77}\text{Nb}_{0.23}\text{O}_2$  sample, which can be attributed to  $\text{Nb}_2\text{O}_5$  (200) STEM elemental mapping (Fig.5) of both  $\text{Ti}_{0.77}\text{Nb}_{0.23}\text{O}_2$  and  $\text{Ti}_{0.97}\text{Nb}_{0.03}\text{O}_2$  show that niobium is mostly evenly distributed in the titania lattice and creates a solid solution. The fact that the  $\text{Nb}_2\text{O}_5$  crystallites cannot be distinguished by XRD neither can be seen in the STEM elemental mapping might be due to their small size (sub 4 nm).

X-ray photoelectron spectroscopy was performed on all 4 samples (0, 1, 5, 10% Nb:TiO<sub>2</sub>), both as surface scans and as depth profiles. For each sample the binding energy for the Ti 2p<sub>3/2</sub> excitation varied between 458.7 and 459.4 eV, which corresponds with Ti<sup>4+</sup> in TiO<sub>2</sub>.<sup>26</sup> Niobium was detected at all levels in all samples. The binding energy for the Nb 3d<sub>5/2</sub> excitation in all samples varied between 207.3 and 207.9 eV, which is representative of Nb<sup>5+</sup> formation. The blue colouration of the as-deposited films suggests the presence of

Ti<sup>3+</sup> and Nb<sup>4+</sup>, though the concentration of reduced species in all the samples is below the detection limit of XPS. Notably the XPS which was based on surface scans only showed one titanium and one niobium environment.

Nb K-edge XANES data are shown in figure 7. Comparison of the XANES data of the films with  $\text{Nb}_2\text{O}_5$  reveal that, while the edge positions are closely similar, the overall features appears to be different to that of  $\text{Nb}_2\text{O}_5$ . This suggests that niobium is in 5+ oxidation state and possibly in two different coordination environments. The Nb K-edge XANES spectra of  $\text{Ti}_{0.97}\text{Nb}_{0.03}\text{O}_2$  and  $\text{Ti}_{0.92}\text{Nb}_{0.08}\text{O}_2$  appears to be closely similar to the one reported earlier by Bhachu *et al.*<sup>27</sup> However, the features of the film containing higher amounts of Nb, in particular the shoulder at ca 18985 and 19019 eV were found to be between the low concentration samples and  $\text{Nb}_2\text{O}_5$ . This suggests that the attempt to increase the amount of Nb in the sample resulted,

probably, in two phases with some amount of  $\text{Nb}_2\text{O}_5$  present in the system. In order to estimate the amount of  $\text{Nb}_2\text{O}_5$  in the samples, we used a linear combination fit (LCF) analysis procedure.

As there are no commercially available standard for niobium doped titania material we assumed that  $\text{Ti}_{0.97}\text{Nb}_{0.03}\text{O}_2$  is a complete solid solution (further proof for this can be seen in the analysis of the EXAFS data) and this therefore was used as one of the reference material and the other was the  $\text{Nb}_2\text{O}_5$  standard.

Results from XANES LCF indicate the presence of two different phases in the as-deposited films. Both  $\text{Ti}_{0.92}\text{Nb}_{0.08}\text{O}_2$  and  $\text{Ti}_{0.77}\text{Nb}_{0.23}\text{O}_2$  films contain niobium doped anatase TiO<sub>2</sub> as well as  $\text{Nb}_2\text{O}_5$ . In the  $\text{Ti}_{0.92}\text{Nb}_{0.08}\text{O}_2$  thin film 10.8 % of the niobium doped in a form of  $\text{Nb}_2\text{O}_5$ . In  $\text{Ti}_{0.77}\text{Nb}_{0.23}\text{O}_2$  thin film there is significantly more niobium (V) oxide phase and is estimated to be ca 48.6 % of the niobium content.

In order to further establish the substitution of Nb in the Ti

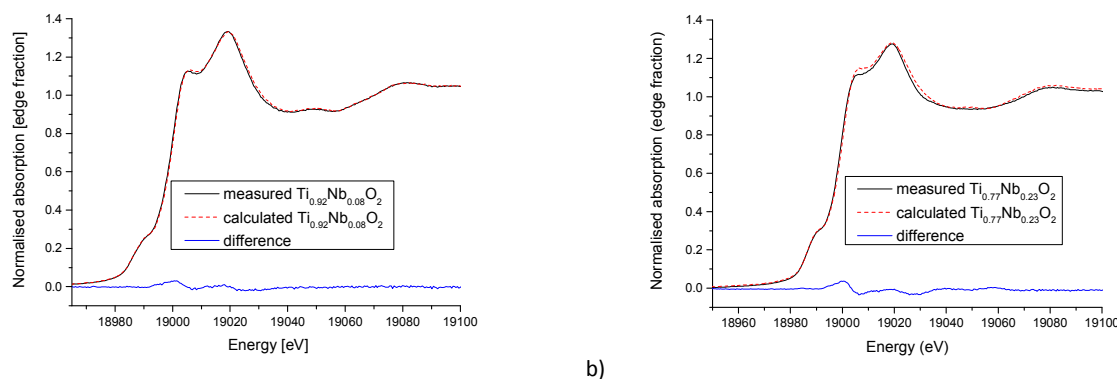


Figure 8. Normalised XANES spectrum along with linear combination of a)  $\text{Ti}_{0.92}\text{Nb}_{0.08}\text{O}_2$  sample containing: 10.8%  $\text{Nb}_2\text{O}_5$  and 89.2% as-deposited  $\text{Ti}_{0.97}\text{Nb}_{0.03}\text{O}_2$  sample and b)  $\text{Ti}_{0.77}\text{Nb}_{0.23}\text{O}_2$  sample containing: 48.4% of  $\text{Nb}_2\text{O}_5$  and 51.6% of as-deposited  $\text{Ti}_{0.97}\text{Nb}_{0.03}\text{O}_2$  sample.

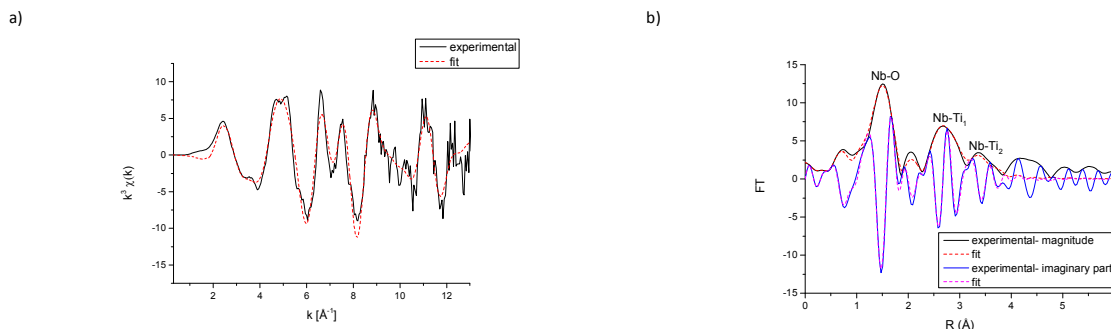


Figure 9. Nb K-edge EXAFS of  $\text{Ti}_{0.97}\text{Nb}_{0.03}\text{O}_2$  thin film a) plot showing the  $k^3\chi(k)$  b) plot showing the magnitude and imaginary part of the Fourier transform of the Nb K-edge EXAFS data of the  $\text{Ti}_{0.97}\text{Nb}_{0.03}\text{O}_2$  thin film.

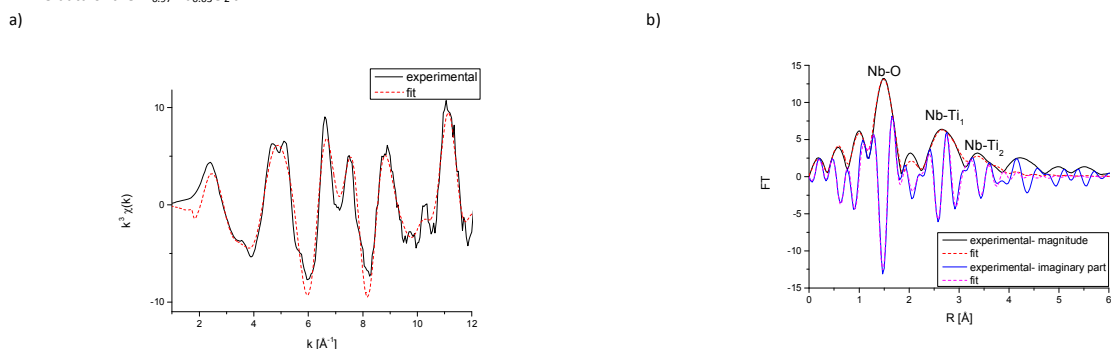


Figure 10. Nb K-edge EXAFS of  $\text{Ti}_{0.92}\text{Nb}_{0.08}\text{O}_2$  thin film a) plot showing the  $k^3\chi(k)$  b) plot showing the magnitude and imaginary part of the Fourier transform of the Nb K-edge EXAFS data of the  $\text{Ti}_{0.92}\text{Nb}_{0.08}\text{O}_2$  thin film.

Table 2. Comparison of % of niobium and titanium in the solution and in the film structure measured by EDX, XANES and XPS. (\*note that in the absence of any Nb substituted  $\text{TiO}_2$  as a model compound, we used this as a reference)

Sample	$\text{Ti}_{0.97}\text{Nb}_{0.03}\text{O}_2$	$\text{Ti}_{0.92}\text{Nb}_{0.08}\text{O}_2$	$\text{Ti}_{0.77}\text{Nb}_{0.23}\text{O}_2$
At. % of Nb in the solution	1	5	10
At. % of Nb in the film (EDX)	3	8	23
At. % of Ti in the film (EDX)	97	92	77
At. % of Nb in the film (XPS)	0.7	1.5	1.0
At. % of Nb doped in the film, that turned into $\text{Nb}_2\text{O}_5$ (XANES)	-*	10.8	48.4

site, we carried out a detailed analysis of the EXAFS data. In pure anatase average interatomic distances of first, second and third neighbours around Ti ions are as follows: Ti – O 1.95 Å, Ti – Ti<sub>1</sub> 3.04 Å and Ti – Ti<sub>2</sub> 3.78 Å.<sup>28</sup> Similarly, in pure niobium (V) oxide the average distances of first, second and third neighbours around Nb ions are as follows: Nb – O 2.01 Å, Nb – Nb<sub>1</sub> 3.39 Å and Nb – Nb<sub>2</sub> 3.60 Å.<sup>29</sup> When niobium is incorporated into the anatase structure the Nb-O distances increase, as niobium has a larger ionic radius (0.064 nm) than titanium (0.0603 nm).<sup>30</sup> Nb K-edge EXAFS data were analysed to yield information about the first, second and third

neighbours and they are presented in Table 1. For the first two samples ( $\text{Ti}_{0.97}\text{Nb}_{0.03}\text{O}_2$  and  $\text{Ti}_{0.92}\text{Nb}_{0.08}\text{O}_2$ ) distances the Nb-O distances are slightly larger compared to average Ti-O distance in Anatase  $\text{TiO}_2$  (1.95 Å) and are Nb – O<sub>1</sub> 1.98 Å for  $\text{Ti}_{0.97}\text{Nb}_{0.03}\text{O}_2$  thin film and Nb – O<sub>1</sub> 1.99 Å, for  $\text{Ti}_{0.92}\text{Nb}_{0.08}\text{O}_2$  thin film. More importantly, the analysis resulted in Nb-Ti distances for the second and third neighbours of ca 3.13Å and 3.85Å for the two Nb doped  $\text{TiO}_2$  films which are significantly different when compared with the structure of  $\text{Nb}_2\text{O}_5$ , which has second neighbour distances of ca 3.39 and 3.6Å. Thus, the slight increase in Nb-O distances and short and long Nb-Ti second neighbour distances (which are similar to the one observed in  $\text{TiO}_2$  anatase structure) suggest Nb ions occupy the Ti site in the anatase  $\text{TiO}_2$  lattice; niobium is known to be highly soluble in titania<sup>31</sup> therefore it is expected to be evenly spread within the material. These distances are marked in the Fourier transform figures 9 and 10 (the data presented is not corrected for the phase shift, but the values given in the table 1 are phase-shift corrected).

EDX analysis (Table 2.) shows that the amount of niobium in the film is higher than the amount added to the solution. For 1 atom % niobium in a solution, the amount incorporated into the film is 3 times higher and is 3 atom %. For 5 atom % niobium in the solution it is 1.5 times higher (8% niobium in a film structure) and for 10 atom % niobium in a solution it is 23 atom % of niobium in the film. The increase in niobium concentration in the films in comparison with its concentration in solution can be explained by the fact that during film

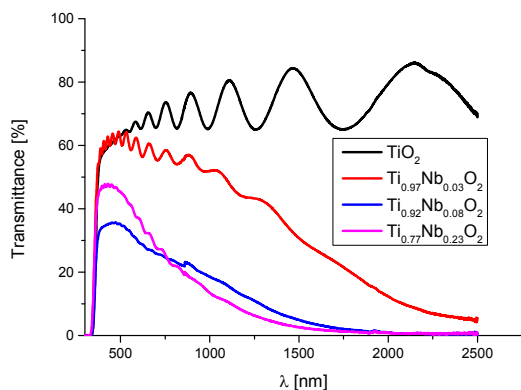


Figure 11. Transmittance (%) plot of as-deposited niobium doped titania thin films over the UV-vis-IR range.

formation, the molecules that undergo diffusion and desorption process are mostly associated with titania. While, the desorption and incorporation rate for titanium is higher, the incorporation rate for niobium species exceeds that of titania, mainly due to the creation of separate,  $\text{Nb}_2\text{O}_5$  phase. Fact that XPS shows very low amounts of niobium on the surface of the film compared to EDX analysis confirms that most niobium is in the bulk and the  $\text{Nb}_2\text{O}_5$  phase occurs mostly not on the surface but in between the doped titania crystals. The thickness of the as-deposited films was derived from the oscillations in the UV-vis spectra by applying the Swanepoel method,<sup>32</sup> which was possible due to the oscillations visible in a figure 11. Thickness of the deposited films is consistent and varies between 1 and 1.5  $\mu\text{m}$ .

From the UV-vis transmittance and reflectance data it can be seen that the transmittance of as-deposited films decrease in the visible region with dopant. Sample  $\text{Ti}_{0.97}\text{Nb}_{0.03}\text{O}_2$  has 60% transmittance in UV-vis region and reaches 0% around 2500 nm, while  $\text{Ti}_{0.92}\text{Nb}_{0.08}\text{O}_2$  and  $\text{Ti}_{0.77}\text{Nb}_{0.23}\text{O}_2$  as-deposited films have respectively 35 and 47% transmittance in UV-vis region and reaches 0% around 1500 nm. It should be noted that the blue films show no change in colour appearance on UV-vis spectra after 6 months in air. The loss of colour requires heating to elevated temperatures (>350°C).

Indirect band gap for each film was determined via the Tauc plot using the  $(\alpha h\nu)^{1/2}$  relation. The results increased from 3.19 eV for pristine anatase  $\text{TiO}_2$ , 3.26 eV for  $\text{Ti}_{0.97}\text{Nb}_{0.03}\text{O}_2$ , 3.35 eV for  $\text{Ti}_{0.77}\text{Nb}_{0.23}\text{O}_2$  to 3.36 eV for  $\text{Ti}_{0.92}\text{Nb}_{0.08}\text{O}_2$  thin film.

The Hall effect studies (Table 3.) on doped films showed that they display *n-type* conductivity as electrons are the prominent type of carrier species. 3 at. % niobium doping into titania lowers sheet resistance to 0.84  $\text{k}\Omega/\square$ , with the highest charge carrier concentration of all films ( $4.6 \times 10^{19} \text{ cm}^{-3}$ ) but the

lowest charge carrier mobility ( $3 \text{ cm}^2/\text{Vs}$ ). Sheet resistance and bulk resistivity were lowest for 8 % niobium doped films and were 0.16  $\text{k}\Omega/\square$  and 0.06  $\Omega\text{cm}$  respectively. Increasing the doping level to 23 % did not lead to a more conductive film, instead the charge carrier concentration was lowest of all the samples examined.

## Discussion

No previous work reports phase segregation in the bulk of as-synthesized Nb:TiO<sub>2</sub> material. As shown in the work of De Trizio et al.<sup>25</sup> there is no evidence of  $\text{Ti}^{3+}$  which is often present in reduced  $\text{TiO}_2$ .<sup>31,33,34</sup> The presence of niobium oxide as a second phase was detected on the surface of niobium doped titania as-synthesized nanocrystals<sup>35,37</sup> and on the surface and near-surface of the air annealed niobium doped titania thin films prepared by the sol-gel method,<sup>19</sup> which is caused by a so called "self-purification" process occurring in most of the doped oxides during the post-treatment due to the mismatch in size of the metal cations.<sup>35,37,38</sup> This paper is first one reporting phase segregation in the Nb:TiO<sub>2</sub> thin film.

Both XRD and Raman analysis reveals the presence of only the anatase phase of TiO<sub>2</sub> which agrees with the work of Kafizas et al.<sup>39</sup> and Bhachu et al.<sup>27</sup> and confirms Hitosugi et al's<sup>41</sup> theory that the presence of niobium atoms as a dopant stabilises the anatase system and inhibits the growth of rutile.<sup>38</sup> Change of the preferred orientation agrees with the work of Bhachu et al. though the majority of publications report unchanged orientation with doping,<sup>26,28,41</sup> which suggests that preferred orientation of thin films depends not only on the amount of doping but also on the method of deposition. Annealing for 12h in air at 500°C results in largely insulating films, which is consistent with existing publications.<sup>40,42,43</sup>

The change in the surface morphology visible in SEM pictures was not previously reported, therefore it might be associated with change in the phase ratio, other than with the amount of niobium incorporated into the lattice.

A comparison of the work presented in this paper with the work of Bhachu et al.<sup>27</sup> suggest that the impact of the structure lies not just between different methods of preparation as LPD, CVD or magnetron sputtering, but the influence on doped TiO<sub>2</sub>'s conductivity also have parameters such as temperature and solvents used for synthesis. Ok et al.<sup>44</sup> suggest that the reason for the higher than expected resistivity is that the grain boundaries in the titania lattice act as the charge carrier traps creating larger shifts in voltage thresholds for bias stress.

Niobium atoms should be evenly distributed within the TiO<sub>2</sub> lattice in order to obtain the highest possible electrical

Table 3. Electrical properties of as-deposited niobium doped titanium dioxide thin films.

Sample	Charge carrier concentration [ $\text{cm}^{-3}$ ]	Charge carrier mobility [ $\text{cm}^2/\text{Vs}$ ]	Bulk resistivity [ $\Omega\text{ cm}$ ]	Resistance [ $\text{k}\Omega/\square$ ]	Film thickness [ $\mu\text{m}$ ]
$\text{Ti}_{0.97}\text{Nb}_{0.03}\text{O}_2$	$4.59 \times 10^{19}$	3.01	0.12	0.84	1.1
$\text{Ti}_{0.92}\text{Nb}_{0.08}\text{O}_2$	$1.23 \times 10^{19}$	10.3	0.06	0.12	1.5
$\text{Ti}_{0.77}\text{Nb}_{0.23}\text{O}_2$	$2.84 \times 10^{18}$	18.9	0.15	0.24	1.1

conductivity<sup>33</sup>, and as STEM elemental mapping shows niobium is largely homogeneously dispersed in the titania particles as big as 0.25- 0.5  $\mu\text{m}$ . It was reported in the literature that the titania lattice can incorporate up to 20 % of niobium ions<sup>30,42</sup> and within that range forms a solid solution with anatase  $\text{TiO}_2$ , while the results obtained from XANES analysis (Table 1.) prove that phase segregation occurs with much smaller amounts of dopant (for 5% Nb in the starting solution there is 10.8% of niobium (V) oxide in the bulk of the film). An alternative explanation is that the deposition by AACVD is under kinetic control and that two pathways exist – one that forms a Nb doped  $\text{TiO}_2$  and another that forms a  $\text{Nb}_2\text{O}_5$  phase with randomly dispersed crystals with size up to 5 nm, which are not detectable by standard resolution XRD nor Raman, but can be only seen on TEM pictures and after close EXAFS analysis. The temperature of the deposition might not be high enough for the diffusion of the niobium oxide into the titania lattice.

Incorporation of niobium into the lattice results in an increase of electrical conductivity, which is a result of extrinsic doping of the niobium ions into the titania. Substituting  $\text{Ti}^{4+}$  by aliovalent  $\text{Nb}^{5+}$  results in introducing additional charge carriers, that improve the bulk conductivity of titania. At the same time increasing phase segregation in the bulk therefore increasing the amount of  $\text{Nb}_2\text{O}_5$  impedes any improvement in conductivity achieved by introducing niobium ions into the lattice (Table 3.). This can be also seen in the band gap correlations. Due to the Burstein-Moss effect electrons populate on the conduction band, causing the optical bandgap to increase<sup>45,46</sup>. The fluctuations in the band gap match variations in the electrical conductivity.

Increasing the amount of  $\text{Nb}_2\text{O}_5$  is visible also in transmittance data. Both  $\text{TiO}_2$  and  $\text{Nb}_2\text{O}_5$  thin films are transparent and colourless. With Nb doping into the lattice,  $\text{TiO}_2$  thin films become blue and transparency both in UV-vis and IR range drops with doping. Though the transparency of  $\text{Ti}_{0.92}\text{Nb}_{0.08}\text{O}_2$  is lower than  $\text{Ti}_{0.77}\text{Nb}_{0.23}\text{O}_2$  which suggest an increasing amount of  $\text{Nb}_2\text{O}_5$  as a second phase present in the film, which also agrees with the results of the Hall effect measurements, EXAFS and TEM.

The results obtained from EXAFS spectra for  $\text{Ti}_{0.97}\text{Nb}_{0.03}\text{O}_2$  and  $\text{Ti}_{0.92}\text{Nb}_{0.08}\text{O}_2$  thin films are consistent with results published by Sacerdoti *et al.*<sup>47</sup> in their study about niobium doped titania thin films deposited by sol-gel and Arbiol *et al.*<sup>36</sup> in their study about niobium doped titania thin films deposited by induced laser pyrolysis. As both groups show in their study niobium in the titanium dioxide anatase lattice is in the  $5^+$  oxidation state.

## Conclusions

Structural properties of niobium doped titanium dioxide films and their impact on electrical and optical properties were investigated. Films were deposited on silica coated glass substrates using aerosol assisted chemical vapour deposition at 500°C. No visible phase segregation was found in XRD nor in Raman, though analysis of the Nb k-edge XANES and EXAFS as well as TEM pictures revealed the presence of niobium both

incorporated into the titanium dioxide lattice as well as present in the form of the  $\text{Nb}_2\text{O}_5$ , which has an impact on the optical and electrical properties as the presence of niobium (V) oxide nanocrystals within titania ones increases resistivity of the film and increases its transparency. Since hexane is compatible with industrial glass manufacture therefore the system we have developed could be used on an industrial scale. The XANES studies suggest that previous literature assignments of niobium doped  $\text{TiO}_2$  should be treated with caution.

## Acknowledgements

Aleksandra J. Gardecka would like to thank Dr. Andreas Kafizas for all the support and useful discussions. We also thank Diamond Light Source for the provision of beam time and Dr. Gianantonio Cibin for his assistance with the measurements.

## References

- 1 L.Sheppard, T. Bak, J. Nowotny, C.C. Sorrel, S. Kumar, A.R. Gerson, M.C. Barnes, C. Ball, *Thin Solid Films*, 2006, **510**, 119-124.
- 2 Kafizas A., Dunnill C.W., Parkin I.P., *J. Mater. Chem.*, 2010, **20**, 8336-8349.
- 3 A. Mills, S. LeHunte, *J. Photochem. Photobiol.*, A, 1997, 108 (1), 1.
- 4 [www.pilkington.com](http://www.pilkington.com)
- 5 H. Tang, K. Prasad, R. Sanjines, P.E. Schmidt, F. Levy, *J. Appl. Phys.* 1994, **75**, 2024.
- 6 T. Minami, *Semicond. Sci. Tech.*, 2005, **20** (1), 35-44.
- 7 P.P. Edwards, A. Porch, M.O. Jones, D.V. Morgan, R.M. Perks, *Dalton Transactions*, 2004, **19**, 2995-3002.
- 8 R.B.H Tahar, T. Ban, Y. Ohya, *J. Appl. Phys. Appl. Phys.*, 1998, **83** (5), 2613-2645.
- 9 K. Ellmer, *J. Phys. D- Appl. Phys.*, 2001, **34**, 3097-3108.
- 10 B.X. Lei, J.X. Liao, R. Zhang, *J. Phys. Chem. C*, 2010, **114**, 15228-15233.
- 11 M.J. Alam, D.C. Cameron, *Thin solid films*, 2000, **377**, 455-459.
- 12 G. Gruner, *J. Mat. Chem.*, 2006, **16** (35), 3533-3539.
- 13 Z.C. Wu, Z.H. Chen, X. Du, *Science*, 2004, **305**, 1273-1276.
- 14 Y. Xu, K. Sheng, Ch. Lich, *ACS Nano*, 2010, **4**, 4324-4330.
- 15 A.L. Dawar, *J. Mater. Chem. Sci.* 1984, **19**, 1.
- 16 Y. Furubayashi, T. Hitosugi, Y. Yamamoto, K. Inaba, G. Kinoda, Y. Hirose, T. Shimada, T. Hasegawa, *Appl. Phys. Lett.*, 2005, **86**, 252101.
- 17 P. Carmichael, Hazafy D., D.S. Bhachu, A. Mills, J.A. Darr, I.P. Parkin, *Phys. Chem. Chem. Phys.*, 2013, **15**, 16788-16794.
- 18 M.R. Antonio, I. Song, H. Yamada, *J. Solid State Chem*, 1991, **93**, 183-192
- 19 A.J. Atanacio, T. Bak, J. Nowotny, *J. Phys. Chem. C*, 2014, **118**, 11174-11185.
- 20 P. Viparelli, P. Ciambelli, J.-C. Volta, J.-M. Herrman, *Appl. Catal A-Gen*, 1999, **182** (1), 165-173.
- 21 A. Kafizas, I. P. Parkin, *J. Chem. Matter.*, 2010, **20**, 2157-2169.
- 22 M. Fehse, S. Cavaliere, P.E. Lippens, I. Savych, A. Iadecola, L. Monconduit, D.J. Jones, J. Roziere, F. Fisher, C. Tessier, L. Stievano, *J. Phys. Chem.*, 2013, **117**, 13827-13835.
- 23 T.D. Manning, I.P. Parkin, C. Blackman, U. Qureshi, *J. Mater. Chem.*, 2005, **15**, 4560-4566.

- 24 S.A. O'Neill, I.P. Parkin, R.J.H. Clark, A. Mills, N. Elliott, *J. Mater. Chem.*, 2003, **13**, 2952-2956.
- 25 L. de Trizio, R. Buonsanti, A.M. Schimpf, A. Llordes, D.R. Gamelin, R. Simountti, D.J. Milliron, *Chem. Mater*, 2013, **25**, 3383-3390.
- 26 W. E. Slink, P. B. DeGroot, *J. Catal.*, 1981, **68**, 423.
- 27 D.S. Bhachu, S. Sathasivam, G. Sankar, D.O. Scanlon, G. Cibin, C.J. Carmalt, I.P. Parkin, G.W. Watson, S.M. Bawaked, A.Y. Obiad, S. Al-Thabaiti, S.N. Basahel, *Adv. Funct. Mater.*, 2014, **24**, 32, 5075-5085.
- 28 M. Horn, C.F. Schwerdtfeger, E.P. Meagher, *Zeitschrift fur Kristallographie*, 1972, **136**, 273-281.
- 29 T.S. Ercit, *Mineralogy and Petrology*, 1991, **43**, 217-223.
- 30 B.N. Joshi, H. Yoon, M.F.A.M. van Hest, S.S. Yoon, *J. Am. Ceram. Soc.*, 2013, **98**, 8, 2623-2627.
- 31 R. Bouchet, A. Weibel, P. Knauth, *Chem. Mater.*, 2003, **15**, 4996-5002.
- 32 R.J. Swanepoel, *J. Phys. E: Sci. Instrum.*, 1983, **16**, 1241.
- 33 M. Hirano, Y.J. Ichihashi, *J. Mater. Sci.*, 2009, **44**, 6135-6143.
- 34 J. Biedrzycki, G. Granozzi, *J. Phys. Chem. C*, 2014, **118**, 8462-8473
- 35 Y. Liu, J.M. Szeifert, J.M. Feckl, B. Mandlmeier, J. Rathousky, O. Hayden, D. Fattakhova-Rohlfing, T. Bein, *ACS Nano*, 2010, **4** (9), 5373-5381.
- 36 J. Arbiol, J. Cerda, G. Dezanneau, A. Cirera, F. Peiro, A. Cornet, J.R. Morante, *J. Appl. Phys.*, 2002, **92**, 853-861.
- 37 F.V. Norris, A.L. Efros, S.C. Erwin, *Science*, 2008, **319**, 1776-1779.
- 38 F.V. Mikulec, M. Kuno, M. Bennati, D.A. Hall, R.G. Griffin, M.G. Bawendi, *J. Am. Chem. Soc.*, 2004, **3**, 787-792
- 39 A. Kafizas, N. Noor, P. Carmichael, D.O. Scanlon, C. J. Carmalt, I. P. Parkin, *Adv. Funct. Mater.*, 2013, 1-5.
- 40 T. Hitosugi, A. Ueda, S. Nakao, N. Yamada, Y. Furubayashi, Y. Hirose, T. Shimada, T. Hasegawa, *Appl. Phys. Lett.*, 2007, **90**, 212106.
- 41 H. Kamisaka, T. Hitosugi, Suenaga T., T. Hasegawa, *J. Chem. Phys.*, 2009, **131**, 034702.
- 42 X. Lu, X. Mou, J. Wu, D. Zhang, L. Zhang, F. Huang, F. Xu, S. Huang, *Adv. Funct. Mater.*, 2010, **20**, 509-515.
- 43 A. Zalewska, *Recent Patents on Engineering*, 2008, **2**, 157-163.
- 44 K.-C. Ok, Y. Park, K.-B. Chung, J.-S. Park, *J. Phys. D: Appl. Phys.*, 2013, **46**, 295102.
- 45 E. Burstein, *Phys. Rev.*, 1954, **96**, 632.
- 46 T.S. Moss, *Proc. Phys. Soc. B.*, 1954, **67**, 775.
- 47 M. Sacerdoti et al., *J. of Solid State Chem.*, 2004, **177**, 1781-1788.